Adaptive Compensation for Power Amplifier Nonlinearity in the Presence of Quadrature Modulation/Demodulation Errors

Young-Doo Kim, Eui-Rim Jeong, *Member, IEEE*, and Yong H. Lee, *Senior Member, IEEE*

***Abstract*—This correspondence proposes techniques that jointly compensate for amplifier nonlinearity and quadrature modulation/demodulation (QM/QDM) errors. The proposed methods are derived based on the polynomial predistortion (PD) employing the indirect learning technique and do not require any additional feedback loop for QM/QDM-error compensation. Compared with the existing joint compensation technique, the proposed methods need some additional parameters to be estimated but exhibit faster convergence and better performance. The advantage of the proposed technique is demonstrated through computer simulation.**

***Index Terms*—Amplifier nonlinearity, digital predistortion, normal-size quadrature modulation/demodualtion errors.**

I. Introduction

Due to the demand for high spectral efficiency in mobile communications, the transmitted signal tends to have a high peak-to-average ratio, and the linearization of a power amplifier (PA) has become an important issue. A popular linearization technique is the baseband digital predistortion (PD) that adaptively adjusts baseband signals depending on the nonlinearity of a PA [1]–[7]. The digital PD methods can be classified into lookup table (LUT) [1]–[3] and polynomial-based methods [4]–[7] according to their implementation: The former approximates the nonlinear PD by a set of piecewise linear functions, and the latter approximates the same by a polynomial. Comparing the two approaches, in general, the LUT methods are simpler to implement, and the polynomial methods exhibit faster convergence.

One difficulty that can be encountered when using a PD technique is its vulnerability to quadrature modulation/demodulation (QM/QDM) errors, including amplitude/phase imbalances and dc offset. For example, it has been observed in [8] that QM errors of only 2% amplitude imbalance, 2° phase imbalance, and 2% dc offset cause about a 30-dB increase of out-of-band spectrum, as compared with no-QM-error cases. To overcome this disadvantage, an extra feedback loop for QM/QDM compensation (QMC/QDMC) is employed in addition to the feedback loop for PD [8]–[12]. This approach is effective but increases hardware cost considerably. The method in [13] jointly compensates for amplifier nonlinearity and QM errors while using only one feedback loop, but it suffers from slow adaptation.

In this correspondence, we propose an alternative method for the joint compensation of amplifier nonlinearity and QM/QDM errors. The proposed method is derived based on the polynomial PD employing the indirect learning technique [5]–[7] and does not need any extra feedback loop for QM/QDM error compensation. In particular, polynomial-based algorithms for jointly performing PD and QM/QDM error compensation are derived, and their parameters are adaptively estimated using recursive least-squares (RLS) algorithms. Compared with the existing joint compensation technique in [13], the proposed methods need some additional parameters to be estimated but exhibit faster convergence and better performance.

This correspondence is organized as follows. In Section II, the proposed joint compensators are derived under the assumption that either QM or QDM errors exist. In Section III, the performance of the proposed methods is examined through computer simulation. Finally, Section IV presents conclusions.

Throughout this correspondence, $(\cdot)^T$, $(\cdot)^H$, and $(\cdot)^*$ denote a transpose, Hermitian transpose, and a complex conjugate, respectively.

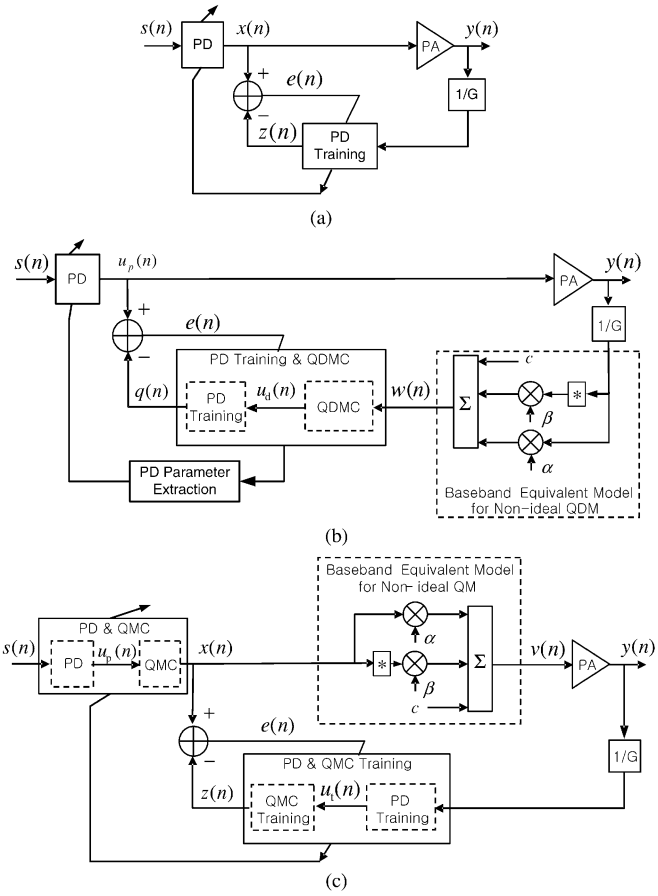

Fig. 1. Baseband equivalent models of a transmitter employing PD with indirect learning. (a) PD when QM and QDM are ideal (no errors). (b) PD when QDM errors exist (ideal QM). (c) Joint PD and QMC when QM errors exist (ideal QDM). Here "*" denotes complex conjugate.

II. Joint PD and QM/QDM Error Compensation

Fig. 1 shows the baseband equivalent models of a transmitter employing digital PD with indirect learning [5], [6]. The following three cases are considered:

1) both QM and QDM are ideal [Fig. 1(a)];
2) QM is ideal, but QDM errors exist [Fig. 1(b)];
3) there are QM errors, but QDM is ideal [Fig. 1(c)].

Manuscript received June 8, 2006; revised December 20, 2006. The associate editor coordinating the review of this manuscript and approving it for publication was Dr. Vitor Heloiz Nascimento. This work was supported by the University Information Technology Research Center Program and by the Brain Korea 21 Project of the Korean government.

Y.-D. Kim is with the Communication Laboratory, Samsung Advanced Institute of Technology, Gyeonggi 440-600, Korea (e-mail: young-doo.kim@samsung.com).

E.-R. Jeong and Y. H. Lee are with the Department of Electrical Engineering and Computer Science, Korea Advanced Institute of Science and Technology, Daejeon 305-701, Korea (e-mail: july@stein.kaist.ac.kr; yohlee@ee.kaist.ac.kr).

Digital Object Identifier 10.1109/TSP.2007.896261

When there are no QM/QDM errors, the parameters of the PD can be directly estimated via the PD training block. Referring to Fig. 1(a), the output of the PD block $x(n)$ is given by

$$x(n) = \mathbf{a}^T(n)\boldsymbol{\phi}(s(n)) \tag{1}$$

where $s(n)$ is a complex-valued input signal $\mathbf{a}(n) = [a_1(n), a_3(n), \ldots, a_{2P+1}(n)]^T$ is the $P+1$-dimensional coefficient vector, and $\boldsymbol{\phi}(s(n)) = [\phi_1(n), \phi_3(n), \ldots, \phi_{2P+1}(n)]^T$ with $\phi_{2p+1}(n) = |s(n)|^{2p}s(n)$ [5], [6]. The coefficients of the PD training block in the feedback path are identical to those of the PD block in the feedforward path, and thus the output $z(n)$ of the training block can be written as

$$z(n) = \mathbf{a}^T(n)\boldsymbol{\phi}(y(n)/G) \tag{2}$$

where G is a positive real number representing the desired gain of a PA. The parameter vector $\mathbf{a}(n)$ can be estimated using the RLS algorithm [5]. When either QM or QDM errors exist, we need QM/QDM error compensators and their trainers. Such processors are derived in the following subsections.

A. PD and QDM Error Compensation

When QDM causes some errors in the feedback path, while QM is ideal, a QDM compensator is placed following the QDM block [Fig. 1(b)]. Then, the parameters of the cascade of QDMC and PD training blocks are adaptively estimated by exploiting a polynomial representing the joint QDMC and PD. In this case, the results of adaptation cannot be directly applied to the feedforward path, which does not have QDMC. Therefore, a processor extracting PD parameters from the results of joint adaptation is employed. Details for deriving the PD and QDMC are presented below.

Let ϵ and θ denote the amplitude and phase imbalances of the QDM. Then, its output $w(n)$ is written as

$$w(n) = \alpha y(n)/G + \beta y^*(n)/G + c \tag{3}$$

where $\alpha = [1+(1+\epsilon)e^{j\theta}]/2$, $\beta = [1-(1+\epsilon)e^{-j\theta}]/2$, and c denotes the dc offset [14], [15]. In (3), $\beta y^*(n)/G$ represents the image signal caused by the I/Q mismatch in QDM. Note that

$$\alpha^* + \beta = 1. \tag{4}$$

In practice, $|\alpha| \approx 1, |\beta| \ll 1$ and $|c| \ll 1$. The QDMC is designed so that $u_d(n) = y(n)/G$, where $u_d(n)$ is the output of the QDMC. The condition for perfect QDMC can be stated as follows.

Observation 1: The QDMC becomes perfect ($u_d(n) = y(n)/G$) if the QDMC output $u_d(n)$ is given by

$$u_d(n) = c_\alpha\, w(n) + c_\beta\, w^*(n) + c_c \tag{5}$$

where $c_\alpha = \alpha^*/(|\alpha|^2 - |\beta|^2)$, $c_\beta = -\beta/(|\alpha|^2 - |\beta|^2)$, and $c_c = (\beta c^* - \alpha^* c)/(|\alpha|^2 - |\beta|^2)$.

This can be proved by using (5) in (3). From (4), it can be shown that the parameters c_α and c_β can be rewritten as

$$c_\alpha = \frac{1 - r^*}{1 - |r|^2} \tag{6a}$$

$$c_\beta = \frac{r - |r|^2}{1 - |r|^2} \tag{6b}$$

where $r = c_\beta/c_\alpha = -\beta/\alpha^*$. Note that, in (5), the QDMC block needs to produce an image signal and dc offset to compensate for the corresponding terms in (6). Based on Observation 1, the QDMC should be expressed as

$$u_{\rm d}(n) = c_1(n)w(n) + c_2(n)w^*(n) + c_3(n) \tag{7}$$

and our objective is to find an adaptive algorithm that makes the coefficient vector $[c_1(n), c_2(n), c_3(n)]$ in (7) converge to $[c_\alpha, c_\beta, c_c]$ in (5).[1] The PD training output $q(n)$ is written as

$$q(n) = \mathbf{a}^T(n)\boldsymbol{\phi}(u_{\rm d}(n)), \tag{8}$$

where $\boldsymbol{\phi}(u_{\rm d}(n)) = [\phi'_1(n), \phi'_3(n), \ldots, \phi'_{2P+1}(n)]$ with

$$\begin{aligned}\phi'_{2p+1}(n) &= |u_{\rm d}(n)|^{2p}u_{\rm d}(n)\\ &= |c_1(n)w(n) + c_2(n)w^*(n)\\ &\quad + c_3(n)|^{2p}(c_1(n)w(n)\\ &\quad + c_2(n)w^*(n) + c_3(n)).\end{aligned} \tag{9}$$

Due to $c_2(n)w^*(n)$ and $c_3(n)$ representing the image and dc offset, respectively, it is difficult to handle $\phi'_{2p+1}(n)$. Fortunately, the image and dc offset are considerably smaller than the desired signal, and thus it is possible to assume that $|c_2(n)| \ll 1$ and $|c_3(n)| \ll 1$ ($|c_1(n)| \approx 1$ due to (4)). Under this assumption, the products of $c_2(n)$ and $c_3(n)$ in (9), such as $|c_2(n)|^2, c_2^2(n), |c_3(n)|^2, c_3^2(n), c_2^*(n)c_3(n)$, and $c_2(n)c_3^*(n)$, can be ignored. After some calculation, $\phi'_{2p+1}(n)$ in (9) can be approximated as

$$\phi'_{2p+1}(n) \approx \mathbf{c}^T_{2p+1}(n)\boldsymbol{\psi}_{2p+1}(w(n)) \tag{10}$$

where

$$\mathbf{c}_{2p+1}(n) = \begin{cases} [c_1(n), c_2(n), c_3(n)]^T, & \text{for } p = 0\\ |c_1(n)|^{2(p-1)}\left[pc_1^2(n)c_3^*(n), (p+1)|c_1(n)|^2c_3(n),\right.\\ \left. pc_1^2(n)c_2^*(n), |c_1(n)|^2c_1(n), (p+1)|c_1(n)|^2c_2(n)\right]^T, & \text{for } p > 0\end{cases}$$

and

$$\boldsymbol{\psi}_{2p+1}(w(n)) = \begin{cases} [w(n), w^*(n), 1]^T & \text{for } p = 0\\ |w(n)|^{2(p-1)}\left[w^2(n), |w(n)|^2, w^3(n),\right.\\ \left. |w(n)|^2w(n), |w(n)|^2w^*(n)\right]^T, & \text{for } p > 0.\end{cases}$$

Now, $q(n)$ in (8) is approximated as

$$\begin{aligned}q(n) &\approx \sum_{p=0}^{P} a_{2p+1}(n)\mathbf{c}^T_{2p+1}(n)\boldsymbol{\psi}_{2p+1}(w(n))\\ &= \sum_{p=0}^{P}\mathbf{g}^T_{2p+1}(n)\boldsymbol{\psi}_{2p+1}(w(n))\\ &= \mathbf{b}^T_{\rm qdm}(n)\psi_{\rm qdm}(w(n))\end{aligned} \tag{11}$$

where $\mathbf{g}_{2p+1}(n) = a_{2p+1}(n)\mathbf{c}_{2p+1}(n)$, $\mathbf{b}_{\rm qdm}(n) = [\mathbf{g}_1^T(n), \ldots, \mathbf{g}_{2P+1}^T(n)]^T$ and $\boldsymbol{\psi}_{\rm qdm}(w(n)) = [\psi_1^T(w(n)), \ldots, \boldsymbol{\psi}_{2P+1}^T(w(n))]^T$. Equation (11) represents the polynomial for joint QDMC and PD. The number of parameters to be determined for the joint operation is $5P+3$, while PD without QDMC requires $P+1$ parameters.[2] To make $q(n)$

[1] Due to (6), $c_1(n)$ and $c_2(n)$ cannot be chosen independently. In fact, $c_2(n)/c_1(n)$ tends to converge to $-\beta/\alpha^*$.

[2] In (11), we may consider directly updating $\{a_{2p+1}(n), c_i(n)\}$ so that the number of parameters for joint PD and QDMC is $P+4$. However, this approach is difficult to follow because of the nonlinearity of $a_{2p+1}(n)$ and $c_i(n)$.

TABLE I
JOINT PD AND QDMC

Initialization:

$\mathbf{\Phi}^{-1}(0) = \delta^{-1}\mathbf{I}, \mathbf{b}_{\mathrm{qdm}}(0) = [1, 0, ..., 0]^T$, and $\mathbf{a}(0) = [1, 0, ..., 0]$,

where δ is a small positive constant.

For each instant of time $n = 1, 2, \cdots$, evaluate

$$\xi_{\mathrm{qdm}}(n) = u_p(n) - \mathbf{b}_{\mathrm{qdm}}^T(n-1)\boldsymbol{\psi}_{\mathrm{qdm}}(w(n))$$
$$= \mathbf{a}^T(n-1)\boldsymbol{\phi}(s(n)) - \mathbf{b}_{\mathrm{qdm}}^T(n-1)\boldsymbol{\psi}_{\mathrm{qdm}}(w(n))$$
$$\mathbf{k}(n) = \frac{\lambda^{-1}\mathbf{\Phi}^{-1}(n-1)\boldsymbol{\psi}_{\mathrm{qdm}}^*(w(n))}{1 + \lambda^{-1}\boldsymbol{\psi}_{\mathrm{qdm}}^T(w(n))\mathbf{\Phi}^{-1}(n-1)\boldsymbol{\psi}_{\mathrm{qdm}}^*(w(n))}$$
$$\mathbf{b}_{\mathrm{qdm}}(n) = \mathbf{b}_{\mathrm{qdm}}(n-1) + \mathbf{k}(n)\xi_{\mathrm{qdm}}(n)$$
$$\mathbf{\Phi}^{-1}(n) = \lambda^{-1}\mathbf{\Phi}^{-1}(n-1) - \lambda^{-1}\mathbf{k}(n)\boldsymbol{\psi}_{\mathrm{qdm}}^T(w(n))\mathbf{\Phi}^{-1}(n-1),$$

where $\xi_{\mathrm{qdm}}(n)$ is a priori estimation error and $\mathbf{k}(n)$ is a gain vector, and obtain $\mathbf{a}(n)$ from $\mathbf{b}_{\mathrm{qdm}}(n)$ using (13)–(15).

close to $u_p(n)$, which is the PD output in the feedforward path, the following LS cost function is defined:

$$J(n) = \sum_{l=1}^{n} \lambda^{n-l} \left| u_p(l) - \mathbf{b}_{\mathrm{qdm}}^T(n)\boldsymbol{\psi}_{\mathrm{qdm}}(w(l)) \right|^2. \quad (12)$$

Before describing the RLS algorithm for obtaining the optimal $\mathbf{b}_{\mathrm{qdm}}^T(n)$ minimizing $J(n)$, it is necessary to derive formulas for extracting $\mathbf{a}(n)$, which represent PD parameters, from $\mathbf{b}_{\mathrm{qdm}}(n)$ [see Fig. 1(b)]. The vector $\mathbf{a}(n)$ is obtained as follows. From (6), $c_1(n)$ and $c_2(n)$ in (7) can be represented as

$$c_1(n) = \frac{1 - \gamma(n)^*}{1 - |\gamma(n)|^2} \quad (13a)$$

$$c_2(n) = \frac{\gamma(n) - |\gamma(n)|^2}{1 - |\gamma(n)|^2} \quad (13b)$$

where $\gamma(n) = c_2(n)/c_1(n)$. If we denote the ith element of $\mathbf{g}_{2p+1}(n)$ in (11) by $g_{2p+1}^{(i)}(n)$, then $\gamma(n)$ can be rewritten as

$$\gamma(n) = g_1^{(2)}(n)/g_1^{(1)}(n). \quad (14)$$

Similarly, it can be seen from the definitions of $\mathbf{g}_{2p+1}(n)$ and $\mathbf{c}_{2p+1}(n)$ that

$$a_{2p+1}(n) = \begin{cases} \dfrac{g_1^{(1)}(n) + g_1^{(2)}(n)}{c_1(n) + c_2(n)}, & \text{for } p = 0 \\ \dfrac{g_{2p+1}^{(4)}(n) + g_{2p+1}^{(5)}(n)}{|c_1(n)|^{2p}(c_1(n) + (p+1)c_2(n))}, & \text{for } p > 0. \end{cases} \quad (15)$$

The vector $\mathbf{a}(n)$ can be evaluated from $\mathbf{b}_{\mathrm{qdm}}(n)$ using (13)–(15). Note that the problem for obtaining $\mathbf{a}(n)$ and $\mathbf{c}_1(n) = [c_1(n), c_2(n), c_3(n)]^T$ from $\{g_{2p+1}^{(i)}(n)\}$ is a nonlinear overdetermined problem,[3] and the method in (13)–(15) is only one of the possible ways for solving this problem. The RLS algorithm for the adaptive PD is described in Table I. Since $\mathbf{b}_{\mathrm{qdm}}(n)$ is a $(5P + 3)$-dimensional vector, each iteration of the RLS algorithm needs $O((5P + 5)^2)$ computations. In addition, extracting PD parameters using (13)–(15) requires $26 + 8P$ real additions and $38 + 16P$ real multiplications.

[3]It is not necessary to compute $c_3(n)$ because joint PD training and QDMC is considered in the feedback path. $c_1(n)$ and $c_2(n)$ are used for evaluating $a_{2p+1}(n)$ in (15).

TABLE II
JOINT PD AND QMC

Initialization:

$\mathbf{\Phi}^{-1}(0) = \delta^{-1}\mathbf{I}$, and $\mathbf{b}_{\mathrm{qm}}(0) = [1, 0, \cdots, 0]^T$,

where δ is a small positive constant.

For each instant of time $n = 1, 2, \cdots$, evaluate

$$\xi_{\mathrm{qm}}(n) = x(n) - \mathbf{b}_{\mathrm{qm}}^T(n-1)\boldsymbol{\phi}_{\mathrm{qm}}(y(n)/G)$$
$$= \mathbf{b}_{\mathrm{qm}}^T(n-1)\left(\boldsymbol{\phi}_{\mathrm{qm}}(s(n)) - \boldsymbol{\phi}_{\mathrm{qm}}(y(n)/G)\right)$$
$$\mathbf{k}(n) = \frac{\lambda^{-1}\mathbf{\Phi}^{-1}(n-1)\boldsymbol{\phi}_{\mathrm{qm}}^*(y(n)/G)}{1 + \lambda^{-1}\boldsymbol{\phi}_{\mathrm{qm}}^T(y(n)/G)\mathbf{\Phi}^{-1}(n-1)\boldsymbol{\phi}_{\mathrm{qm}}^*(y(n)/G)}$$
$$\mathbf{b}_{\mathrm{qm}}(n) = \mathbf{b}_{\mathrm{qm}}(n-1) + \mathbf{k}(n)\xi_{\mathrm{qm}}(n)$$
$$\mathbf{\Phi}^{-1}(n) = \lambda^{-1}\mathbf{\Phi}^{-1}(n-1) - \lambda^{-1}\mathbf{k}(n)\boldsymbol{\phi}_{\mathrm{qm}}^T(y(n)/G)\mathbf{\Phi}^{-1}(n-1)$$

B. PD and QM Error Compensation

The proposed processor that jointly performs PD and QM error compensation is illustrated in Fig. 1(c). To compensate for QM errors, a QMC block is located right after the PD block. Then, in the feedback path, PD training is cascaded with QMC training. In this case, the parameters obtained from the training block can be directly applied to the PD and QMC block in the feedforward path. Based on Observation 1, the QMC is modeled as

$$x(n) = d_1(n)u_{\mathrm{p}}(n) + d_2(n)u_{\mathrm{p}}^* + d_3(n) \quad (16)$$

where $u_p(n)$ is the PD output. Since $u_p(n) = \mathbf{a}^T(n)\boldsymbol{\phi}(s(n))$, where $\mathbf{a}(n)$ is the PD parameter vector in (1), $x(n)$ in (16) is rewritten as

$$x(n) = d_1(n)\mathbf{a}^T(n)\boldsymbol{\phi}(s(n)) + d_2(n)\mathbf{a}^H(n)\boldsymbol{\phi}^*(s(n)) + d_3(n)$$
$$\triangleq \mathbf{b}_{\mathrm{qm}}^T(n)\boldsymbol{\phi}_{\mathrm{qm}}(s(n)) \quad (17)$$

where $\mathbf{b}_{\mathrm{qm}}(n)$ and $\boldsymbol{\phi}_{\mathrm{qm}}(s(n))$ are $2P + 3$-dimensional parameter vectors given by $\mathbf{b}_{\mathrm{qm}}(n) = [d_1(n)\mathbf{a}^T(n), d_2(n)\mathbf{a}^H(n), d_3(n)]^T$ and $\boldsymbol{\phi}_{\mathrm{qm}}(s(n)) = [\boldsymbol{\phi}^T(s(n)), \boldsymbol{\phi}^H(s(n)), 1]^T$. Equation (17) represents the polynomial for joint PD and QMC. In this case, it is necessary to determine $2P + 3$ parameters. The coefficients of the PD and QMC training blocks in the feedback path are identical to those of the PD and QMC blocks in the feedforward path, and thus the output $z(n)$ of the training block can be written as

$$z(n) = \mathbf{b}_{\mathrm{qm}}^T(n)\boldsymbol{\phi}_{\mathrm{qm}}(y(n)/G). \quad (18)$$

Since $z(n)$ in (18) has the standard linear form, an LS cost function can be defined as in (12), and an RLS algorithm for recursively evaluating $\mathbf{b}_{\mathrm{qm}}(n)$ can be derived. This algorithm is described in Table II. In this case, the number of parameters to be estimated in the RLS algorithm is $2P + 3$, and no additional computations are needed after the RLS recursion. Therefore, the joint PD and QMC needs less computation than the joint PD and QDMC.

III. SIMULATION RESULTS

Computer simulations were conducted to examine the performance of the proposed schemes. In the simulations, the following parameters are assumed: 16-QAM signal constellation is used for transmission; the pulse-shaping filter is the 8-times oversampled raised-cosine filter with a roll-off factor 0.22; the forgetting factor λ is 0.95; and δ is $1/1000$. As specified in Tables I and II, the initial estimates of $\mathbf{b}_{\mathrm{qdm}}(n)$, $\mathbf{a}(n)$ and $\mathbf{b}_{\mathrm{qm}}(n)$ are given by $\mathbf{b}_{\mathbf{qdm}}(0) = [1, 0, \ldots, 0]^T$,

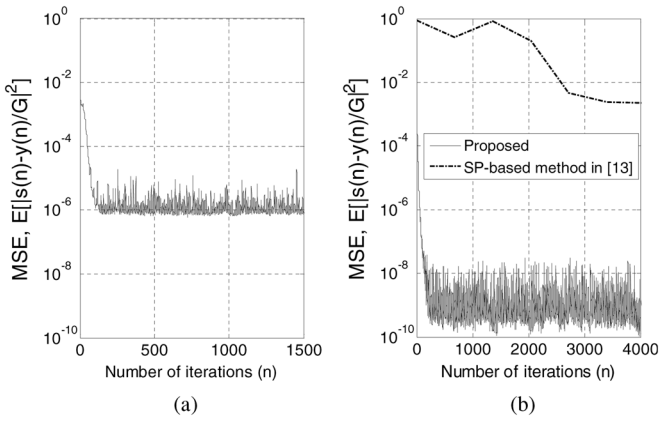

Fig. 2. Learning curves consisting of the MSEs between the input $s(n)$ and the PA output $y(n)$ of the proposed systems. (a) PD and QDM error compensation [Fig. 1(b)]. (b) Joint PD and QMC [Fig. 1(c)].

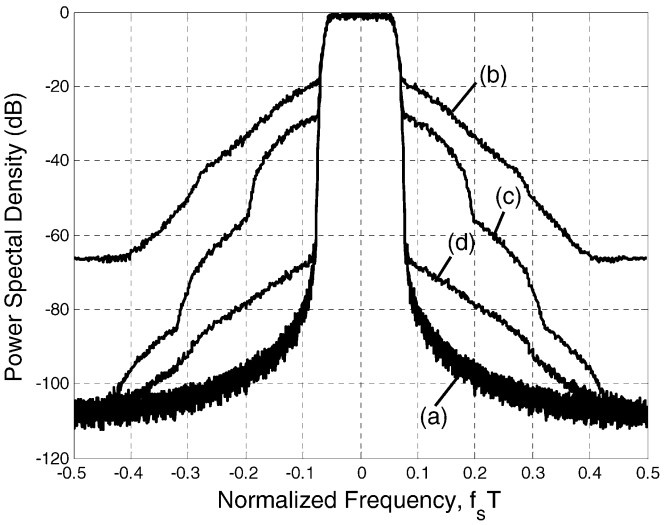

Fig. 3. Power spectral density of the PA output $y(n)$ when QDM errors exist. (a) Ideal case (PSD of $s(n)$). (b) System employing PD but no QDMC [Fig. 1(a)]. (c) System employing neither PD nor QDMC. (d) Proposed system [Fig. 1(b)].

$\mathbf{a}(0) = [1, 0, \ldots, 0]^T$, and $\mathbf{b}_{\rm qm}(0) = [1, 0, \ldots, 0]^T$. For these initial values, the proposed algorithms exhibited convergence. The amplitude and phase imbalances and dc offset for the QM and QDM are identical: $\epsilon = 0.03$ and $\theta = 3^\circ$, which correspond to $\alpha = 1.0143 + j\,0.027$ and $\beta = -0.0143 + j\,0.027$. The dc offset is given by $c = 0.03 + j\,0.01$. The PA input $v(n)$ and output $y(n)$ are assumed to obey the Saleh model [17] given by

$$y(n) = \frac{1.1|v(n)|}{1 + 0.3|v(n)|^2} \exp\left[j\left(\angle v(n) + \frac{|v(n)|^2}{1 + |v(n)|^2}\right)\right].$$

The linearized gain G is set to one $(G = 1)$, and the peak back-off (PBO) is set to 1.5 dB. The PD with a polynomial order $P = 3$ is employed. For comparison, the method in [13], which performs joint PD and QMC, is also considered. (For the case of joint PD and QDMC, only the proposed algorithm is examined because there exists no alternative scheme.) This method estimates the PD and QMC parameters from an estimate of the out-of-band signal power (SP) and is referred to as the SP-based method. In the simulation, following the suggestion in [13], the PD and QMC parameters are updated whenever 700 samples of out-of-band signal power are collected.

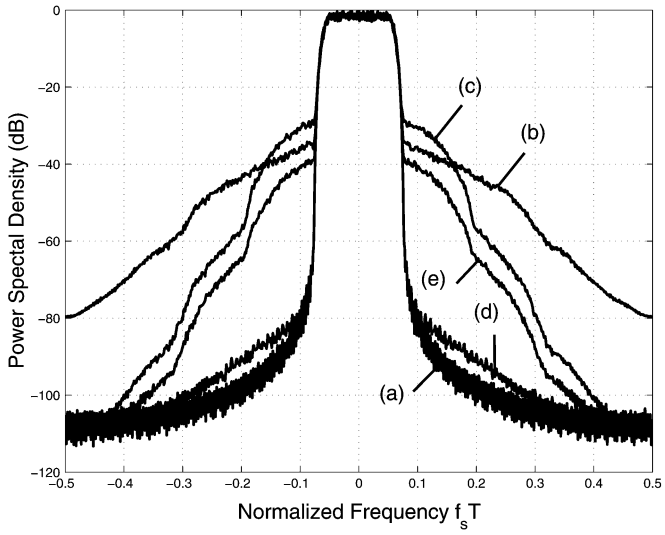

Fig. 4. Power spectral density of the PA output $y(n)$ when QM errors exist. (a) Ideal case (PSD of $s(n)$). (b) System employing PD but no QMC [Fig. 1(a)]. (c) System employing neither PD nor QMC. (d) Proposed system [Fig. 1(c)]. (e) SP-based method in [13].

The learning curves showing the mean-square errors (MSEs) between the input $s(n)$ and the PA output $y(n)$ are shown in Fig. 2 (these are obtained through 1 000 independent trials). Both the proposed systems [Fig. 1(b) and (c)] converge to a steady state after about 150 iterations (or, equivalently, 150 sample periods),[4] while the SP-based method starts to converge after 2800 sample periods. In Fig. 2(b), the MSEs of the SP-based method are considerably larger than those of the proposed scheme. Comparing the steady-state MSEs of the two proposed methods, the system with QDMC results in larger MSE than that with QMC. This happens for the following reasons. First, the number of parameters for the QDMC and PD training $(5P + 3)$ is larger than that for PD and QMC training $(2P + 3)$, and the PD parameter extraction is needed for the system with QDMC. Second, the derivation of the joint QDMC and PD training is based on the approximation in (10), while the joint PD training and QMC is derived without any approximation.

Figs. 3 and 4 show the output power spectral densities (PSDs) of the proposed systems with QDMC and QMC, respectively. For comparison, the PSD of the input $s(n)$, the output PSD of the system in Fig. 1(a) (PD without QDMC/QMC) and that of the system employing neither PD nor QDMC/QMC are also shown. For both cases (QDMC and QMC), the out-of-band PSDs of the proposed systems are considerably lower than those of the other systems—in fact, the former are reasonably close to the PSD of the input $s(n)$, particularly for the system with QMC. The system in Fig. 1(a) (PD without QDMC/QMC) results in out-of-band PSDs, which are even higher than those from the system without any adaptive processing. This indicates that the adaptive PD should be used in conjunction with QDMC/QMC when QDM/QM errors are not negligible. In Fig. 4, the SP-based method exhibits only minor performance gain, as compared with the system employing neither PD nor QMC.

IV. Conclusion

Polynomial-based adaptive methods for jointly compensating amplifier nonlinearity and QM/QDM errors have been proposed. These were derived for the adaptive PD system with indirect learning technique under the assumption that either QM or QDM errors exist. It

[4]It was observed that the conventional PD in Fig. 1(a), which operates with ideal QM and QDM, also needed about 150 iterations for convergence.

was observed that the design and implementation of PD in the presence of QDM errors is more difficult than those of PD in the presence of QM errors. Computer simulation results demonstrated that the proposed schemes can suppress out-of-band PSD significantly. We will conduct further research in this direction that will include the design of adaptive PD when both QM and QDM errors exist.

REFERENCES

[1] J. K. Cavers, "Amplifier linearization using a digital predistorter with fast adaptation and low memory requirements," *IEEE Trans. Veh. Technol.*, vol. 39, no. 4, pp. 374–382, Nov. 1990.

[2] A. S. Wright and W. G. Curtler, "Experimental performance of an adaptive digital linearized power amplifier," *IEEE Trans. Veh. Technol.*, vol. 41, no. 4, pp. 395–400, Nov. 1992.

[3] K. J. Muhonen, M. Kavehrad, and R. Krishnamoorthy, "Look-up table techniques for adaptive digital predistortion: A development and comparison," *IEEE Trans. Veh. Technol.*, vol. 49, no. 5, pp. 1995–2002, Sep. 2000.

[4] E. Biglieri, S. Barberis, and M. Catena, "Analysis and compensation of nonlinearities in digital transmission systems," *IEEE J. Sel. Areas. Commun.*, vol. 6, no. 1, pp. 42–51, Jan. 1988.

[5] R. Marsalek, P. Jardin, and G. Baudoin, "From post-distortion to predistortion for power amplifiers linearization," *IEEE Commun. Lett.*, vol. 7, no. 7, pp. 308–310, Jul. 2003.

[6] R. Raich, H. Qian, and G. T. Zhou, "Orthogonal polynomials for power amplifier modeling and predistorter design," *IEEE Trans. Veh. Technol.*, vol. 53, no. 5, pp. 1468–1479, Sep. 2004.

[7] L. Ding, G. T. Zhou, D. R. Morgan, Z. Ma, S. Kenney, J. Kim, and C. R. Giardina, "A robust digital baseband predistorter constructed using memory polynomials," *IEEE Trans. Commun.*, vol. 52, no. 1, pp. 159–165, Jan. 2004.

[8] J. K. Cavers and M. W. Liao, "Adaptive compensation for imbalance and offset losses in direct conversion transceivers," *IEEE Trans. Veh. Technol.*, vol. 42, no. 4, pp. 581–588, Nov. 1993.

[9] M. Faulkner, T. Mattsson, and W. Yates, "Automatic adjustment of quadrature modulators," *Electron. Lett.*, vol. 27, no. 3, pp. 214–216, Jan. 1991.

[10] J. K. Cavers, "New methods for adaptation of quadrature modulators and demodulators in amplifier linearization circuits," *IEEE Trans. Veh. Technol.*, vol. 46, no. 3, pp. 707–716, Aug. 1997.

[11] M. Faulkner and M. Johansson, "Adaptive linearization using predistortion—experimental results," *IEEE Trans. Veh. Technol.*, vol. 43, no. 2, pp. 323–332, May 1994.

[12] A. Lohtia, P. Goud, and C. Englefield, "An adaptive digital technique for compensating for analog quadrature modulator/demodulator impairments," *Proc. IEEE Pacific Rim Conf.*, pp. 447–450, 1993.

[13] D. S. Hilborn, S. P. Stapleton, and J. K. Cavers, "An adaptive direct conversion transmitter," *IEEE Trans. Veh. Technol.*, vol. 43, no. 2, pp. 223–233, May 1994.

[14] J. K. Cavers, "The effect of quadrature modulator and demodulator errors on adaptive digital predistorters for amplifier linearization," *IEEE Trans. Veh. Technol.*, vol. 46, no. 2, pp. 456–466, May 1997.

[15] I. H. Sohn, E. R. Jeong, and Y. H. Lee, "Data-aided approach to I/Q mismatch and DC offset compensation in communication receivers," *IEEE Commun. Lett.*, vol. 6, no. 12, pp. 547–549, Dec. 2002.

[16] G. T. Gil, I. H. Sohn, J. K. Park, and Y. H. Lee, "Joint ML estimation of carrier frequency, channel, I/Q mismatch, and DC offset in communication receivers," *IEEE Trans. Veh. Technol.*, vol. 54, no. 1, pp. 338–349, Jan. 2005.

[17] A. M. Saleh, "Frequency-independent and frequency-dependent nonlinear models of TWT amplifiers," *IEEE Trans. Commun.*, vol. 29, no. 11, pp. 1715–1720, Nov. 1981.

Using Spatial Diversity to Detect Narcotics and Explosives Using NQR Signals

Andreas Jakobsson, *Senior Member, IEEE*, and Magnus Mossberg, *Member, IEEE*

***Abstract*—Nuclear quadrupole resonance (NQR) offers an unequivocal method of detecting hidden narcotics and explosives. Unfortunately, the practical use of NQR is restricted by the low signal-to-noise ratio (SNR) and means to improve the SNR are vital to enable a rapid, reliable and convenient system. In this correspondence, we develop two multichannel detectors to counter the typically present radio frequency interference. Numerical simulations indicate that the proposed methods offers a significantly improved robustness to uncertainties in the parameters detailing the examined sample.**

***Index Terms*—Land mine detection, maximum-likelihood detection, multidimensional signal processing, nuclear quadrupole resonance, radio frequency spectroscopy.**

I. INTRODUCTION

Nuclear quadrupole resonance (NQR) is a radio frequency (RF) technique offering an unequivocal method of detecting the presence of quadrupolar nuclei, such as the nitrogen isotope ^{14}N, prevalent in many forms of high explosives, narcotics, and drugs. Recently, the technique has received increasing attention as an important method for detecting land mines. This is because the NQR signal offers a unique signature, differentiating it from most other mine detection techniques that suffer from trying to detect non-unique features, such as the presence of metal. Further, NQR is also of particular interest due to the possibility of using the technique to detect explosives and/or narcotics at airports and other public places. Recent studies show that the unique NQR signature can offer a high probability of detection for a given false alarm rate (see [1]–[8] and the references therein). The observed NQR frequencies depend on the interaction between the electric quadrupole moment of the nucleus and the electric field gradient generated at the nuclear site by external charges [9]. Because of its high specificity, there is little or no interference from other nitrogen-containing material that may be present. However, due to the used band of excitation frequencies, the NQR signals are typically prone to strong RF interference (RFI). In the recent literature (see, e.g., [3], [10], and [11]), several approaches for interference cancellation using a set of additional antennas, aimed at measuring only the contribution of the interference signal, have been proposed. Typically, such approaches will significantly improve the signal-to-noise ratio (SNR) but will not succeed in fully removing the influence of the interference. As a result, the applied detection algorithm should be constructed to be robust to residual RFI. The commonly applied methods, primarily based on linear filtering via the fast Fourier transform (FFT) or on matched filtering assuming a reliable estimate of the parameters describing the examined sample, such as the temperature of the target, do not include such robustness. Furthermore,

Manuscript received June 19, 2006; revised January 19, 2007. The associate editor coordinating the review of this manuscript and approving it for publication was Dr. A. Rahim Leyman. This work was supported in part by Carl Trygger's Foundation and the Swedish Research Council. Parts of this correspondence first appeared in the *Proceedings of the IEEE Workshop on Sensor Array and Multichannel Signal Processing*, Waltham, MA, July 12–14, 2006, pp. 79–83.

The authors are with the Department of Electrical Engineering, Karlstad University, SE-651 88 Karlstad, Sweden (e-mail: andreas.jakobsson@ieee.org; magnus.mossberg@kau.se).

Digital Object Identifier 10.1109/TSP.2007.896287